Article

Th17, Th22, and Myeloid-Derived Suppressor Cell Population Dynamics and Response to IL-6 in 4T1 Mammary Carcinoma

Viva J. Rasé [1,2], Reid Hayward [3] , James M. Haughian [1] and Nicholas A. Pullen [1,*]

1   School of Biological Sciences, University of Northern Colorado, Greeley, CO 80639, USA
2   Department of Pathology, University of Utah School of Medicine, Salt Lake City, UT 84112, USA
3   School of Sport and Exercise Science, University of Northern Colorado, Greeley, CO 80639, USA
*   Correspondence: nicholas.pullen@unco.edu; Tel.: +1-970-351-1843; Fax: +1-970-351-2335

Abstract: Immunotherapies relying on type 1 immunity have shown robust clinical responses in some cancers yet remain relatively ineffective in solid breast tumors. Polarization toward type 2 immunity and expansion of myeloid-derived suppressor cells (MDSC) confer resistance to therapy, though it remains unclear whether polarization toward type 3 immunity occurs or has a similar effect. Therefore, we investigated the involvement of type 3 Th17 and Th22 cells and their association with expanding MDSC populations in the 4T1 mouse mammary carcinoma model. Th17 and Th22 were detected in the earliest measurable mass at d 14 and remained present until the final sampling on d 28. In peripheral organs, Th17 populations were significantly higher than the non-tumor bearing control and peaked early at d 7, before a palpable tumor had formed. Peripheral Th22 proportions were also significantly increased, though at later times when tumors were established. To further address the mechanism underlying type 3 immune cell and MDSC recruitment, we used CRISPR-Cas9 to knock out 4T1 tumor production of interleukin-6 (4T1-IL-6-KO), which functions in myelopoiesis, MDSC recruitment, and Th maturation. While 4T1-IL-6-KO tumor growth was similar to the control, the reduced IL-6 significantly expanded the total CD4+ Th population and Th17 in tumors, while Th22 and MDSC were reduced in all tissues; this suggests that clinical IL-6 depletion combined with immunotherapy could improve outcomes. In sum, 4T1 mammary carcinomas secrete IL-6 and other factors, to polarize and reshape Th populations and expand distinct Th17 and Th22 populations, which may facilitate tumor growth and confer immunotherapy resistance.

Keywords: type 3 immunity; MDSC; IL-22; cancer

1. Introduction

Immune checkpoint therapies targeting CTLA-4 and PD-1/PD-L1 have shown clinical success in hematological tumors and solid tumors with a high neoantigen burden, leading to tumor regression and considerable gains in patient survival [1–5]. Unfortunately, not all patients benefit equally from checkpoint inhibition as non-responders or poor responders, adverse immune events, and tumor hyper-progression have also been reported [6–10]. The reports of hyper-progression suggest, paradoxically, that releasing checkpoint controls on the immune system can aid in tumor progression in some immunological circumstances. These undesirable outcomes clearly indicate a need to understand better the cancer patient's immunological status, to ensure that checkpoint and other immunotherapies are delivered into a well-defined and optimally effective immune context.

Tumor responses to checkpoint immunotherapy are undoubtedly influenced by the phenotype and quantity of localized tumor infiltrating lymphocytes (TILs) [11], and the type 1 Th1 cell phenotype is generally accepted as the most effective coordinator against tumor cells in this locale, as it works in conjunction with most current immunotherapy treatments [12,13]. However, it is now clear that tumors signal beyond their physical boundaries and release systemic factors that mitigate the type 1 T cell response and foster

immune responses beneficial to the tumor. For example, tumors may secrete G-CSF, M-CSF, or IL-6 cytokines to dysregulate myelopoiesis and promote the production of immune inhibitory cells, such as MDSC, that impair CD8$^+$ cytotoxic T cell activation and more broadly inhibit type 1 effector T$_h$ cell function [14].

Another mode of systemic immune evasion is tumor-dependent immune polarization that attenuates the type 1 response and intensifies the potentially tumor-promoting type 2 or type 3 T$_h$ response [15–18]. Evidence from preclinical models such as MMTV-PyMT mammary and other cancer types indicates that tumors can skew T cell populations toward a helminth-targeting type 2 (T$_h$2 cell-mediated) response [19–21]. Similarly, T cell polarization toward a T$_h$17- or T$_h$22-cell-mediated type 3 response that would normally combat microbial infection has been observed in mouse models and human cases of cervical, ovarian, prostate, and gastric cancers [16,22–27]. Specifically in mammary carcinoma, IL-22, a cytokine produced in large quantities by T$_h$22, has been shown to exacerbate tumor growth [28]. Intriguingly, polarization toward type 3 immunity in other conditions, including *H. pylori* infection and autoimmune disease (lupus erythematosus, encephalomyelitis, arthritis), arises concurrently with elevated MDSC [29–31], which is a well-described feature of many breast malignancies [32]. To our knowledge, no studies of mammary carcinoma have addressed the association between type 3 immunity and MDSC.

Mammary carcinomas stand to benefit from type 3 immune polarization. The polarization toward type-3-immune T$_h$17 requires the presence of TGFβ-1, IL-6, and IL-23; alternatively, T$_h$22 requires the combination of IL-6, IL-23, and IL-1β [33]. The expansion of class-defining T$_h$17 or T$_h$22 helper cells could locally and systemically increase concentrations of the cytokines IL-17A and IL-22, respectively [34]. The chronic presence of these type 3 cytokines has been linked to increased tumor growth, enhanced tumor cell survival, and metastatic potential [25,35,36]. Similarly, knocking out the IL-17 receptor in the 4T1 model heightened apoptosis and slowed tumor cell proliferation [37]. Mechanistically, IL-6 is implicated in both MDSC recruitment and T$_h$17/ T$_h$22 polarization [33,38], yet no studies have explored whether chronic overexpression of IL-6 from a developing tumor may, in fact, elicit both MDSC and type 3 T$_h$ expansion in the context of mammary carcinoma.

The present study examines the response of type 3 T helper populations T$_h$17 and T$_h$22, along with transitional T$_h$1/17 [39], in the 4T1 model of mouse mammary carcinoma. The 4T1 model shares similarities with metastatic triple-negative breast cancers that are resistant to checkpoint immunotherapy [40,41]. Moreover, 4T1 tumors elicit a pronounced myeloid reaction in the form of MDSC [42], which are regulated by IL-6 [43]. Thus, this system enabled the characterization of IL-6 and its role in co-regulating T helper and MDSC immunity. Our findings suggest there is a robust, IL-6-dependent polarization toward type 3 immunity, which accompanies MDSC expansion in this mammary carcinoma model, and that this altered T$_h$ cell landscape should be considered to improve immune and other oncotherapies.

2. Results

2.1. T$_h$ Populations in Response to 4T1-WT Tumors

Tumors and spleen. Following injection of 10^4 4T1 carcinoma cells into the mammary glands of BALB/cJ mice, small palpable tumors formed at the injection site by d 14, and by ~d 28 tumors approached the maximum humane dimension allowable under our IACUC protocol (Figure 1A,B). During this course of tumor development, we also measured spleen mass, as reports have indicated splenomegaly is associated with late-stage, established 4T1 tumors [44]. Unexpectedly, at d 7, before there was a palpable tumor, we observed a significant reduction in spleen mass relative to the controls (Figure 1C). As the tumors became larger and more established (d 21 and 28), the tumor-bearing animals showed a pronounced increase in spleen size, consistent with what has been reported elsewhere. To our knowledge, this is the first report of an early reduction in spleen size in the 4T1 tumor model, which will require further studies to determine the underlying cause.
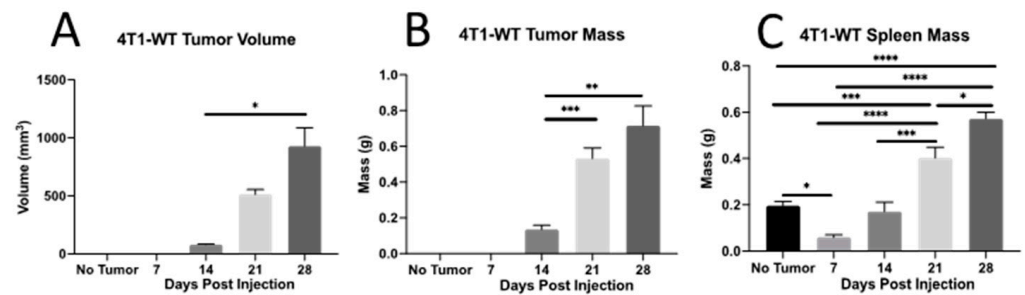
Figure 1. Tumor and spleen sizes in 4T1 tumor-bearing animals. The 4T1-WT mammary carcinoma cells (10^4) were engrafted into the mammary gland of BALB/cJ mice, and animals were assessed for (**A**) tumor volume, (**B**) tumor mass, and (**C**) spleen mass at the times indicated. Data are represented as mean $\pm$ SEM; n = 4–11 mice per time point. * $p < 0.05$, ** $p < 0.01$, *** $p < 0.001$, and **** $p < 0.0001$.

Total CD4$^+$ T$_h$ cell populations. Using the gating strategy outlined in Figure 2, we initially assessed T$_h$-immune cell populations in the spleen, blood, bone marrow, and tumor (when possible) at various stages of wild-type 4T1 (4T1-WT) mammary tumor development (Figure 3). The percentage of total CD4$^+$ T$_h$ cells remained relatively unchanged in the tumor, blood, and other peripheral tissues, with modest increases detected in the spleen and bone marrow at d 14 and 21, respectively (Figure 3A,B).

Type 3 T$_h$ cell populations. While the total T$_h$ cell population showed only modest changes over time, we observed dynamic changes in the T$_h$ cell subtypes for type 1 and type 3 immunity. Both type 3 T$_h$17 and T$_h$22 cells were present in the tumor at all time points, where there was sufficient tissue to assess, with T$_h$17 significantly declining over time, whereas T$_h$22 increased in the tumor tissue (Figure 3D,F). Interestingly, in the spleen, the T$_h$17 population increased significantly by d 7 post-4T1 injection (before a palpable tumor was detectable) and declined thereafter, such that the percentage of T$_h$17 remaining by 28 d was significantly lower than in the control animals. This same trend in early T$_h$17 recruitment and later decline was also observed in the blood and bone marrow (Figure 3C). Notably, the T$_h$22 populations moved independently of T$_h$17 and were not expanded at early time points in peripheral organs. T$_h$22 showed a delayed increase and was only elevated at later time points, a pattern most prominent in the blood (Figure 3E). Intrigued by this inverse pattern of T$_h$17 and T$_h$22 recruitment, we computed the Pearson correlation between T$_h$22 and T$_h$17 recruitment in the various tissues over time. There was no correlation between T$_h$22 and T$_h$17 in the blood or bone marrow; however, there was a significant negative correlation ($r^2 = 0.14$, $p < 0.05$) in the spleen and a significant positive correlation associated with their coexistence in tumors ($r^2 = 0.25$, $p < 0.05$; Figure 3A–D).

T$_h$1 polarization. We also assessed T$_h$1 recruitment, as type 1 immunity is centrally involved in cancer immunotherapies. In the blood (Figure 4G, center panel), T$_h$1 was significantly expanded across all times post-injection, consistent with a mobilization of this T$_h$ subtype in response to a neoplastic threat; however, this peaked early at d 7 and declined thereafter. A similar pattern was observed in bone marrow, except that the peak occurred at d 14 (Figure 4G, right panel). T$_h$1 was likely mobilizing from the spleen, as proportions there were below controls at d 7, but then later recovered (Figure 4G, left panel). Interestingly, T$_h$1 is present in the tumor, though the proportions did not significantly increase along with the peripheral rise in T$_h$1, suggesting unknown tumor-specific mechanisms that were preventing infiltration of these cells into the tumor microenvironment (Figure 4H).
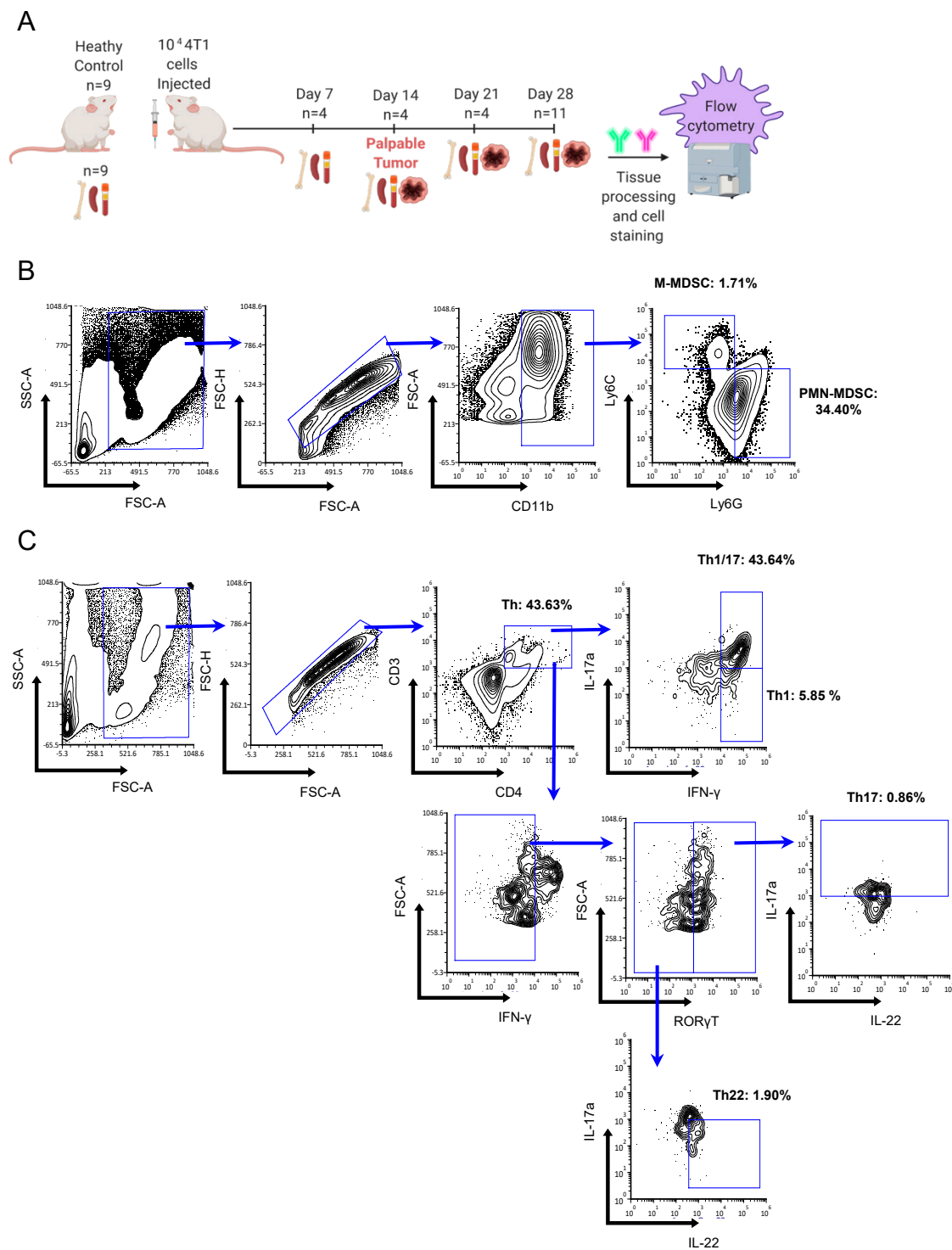
Figure 2. Time-course methodology and flow cytometry gating strategy. (**A**) Wild type 4T1 (4T1-WT, 10^4 cells) were injected into syngeneic BALB/cJ mice and spleen, blood, bone marrow, and tumor (when present) and were harvested 7, 14, 21, and 28 days later. The 4T1 mice formed palpable tumors 14 d after injection. Tissue was processed, stained, and analyzed by flow cytometry, with age-matched healthy non-tumor-bearing mice included for comparison. Representative blood sample shows gating strategies for (**B**) MDSC subtypes M-MDSC (CD11b$^+$Ly-6G$^-$Ly-6C^{hi}) and PMN-MDSC (CD11b$^+$Ly-6G$^+$Ly-6C^{low}) as well as (**C**) CD3$^+$CD4$^+$ T helper (T$_h$) subtypes T$_h$1 (CD3$^+$CD4$^+$IFN-γ^+RORγt$^-$IL-17A$^-$IL-22$^{+/-}$), T$_h$1/17 (CD3$^+$CD4$^+$RORγt$^+$IFN-γ^+IL-17A$^+$IL-22$^{+/-}$), T$_h$17 (CD3$^+$CD4$^+$RORγt$^+$IFN-γ^-IL-17A$^+$IL-22$^{+/-}$), and T$_h$22 (CD3$^+$CD4$^+$IFN-γ^-RORγt$^-$IL-17A$^-$IL-22$^+$).
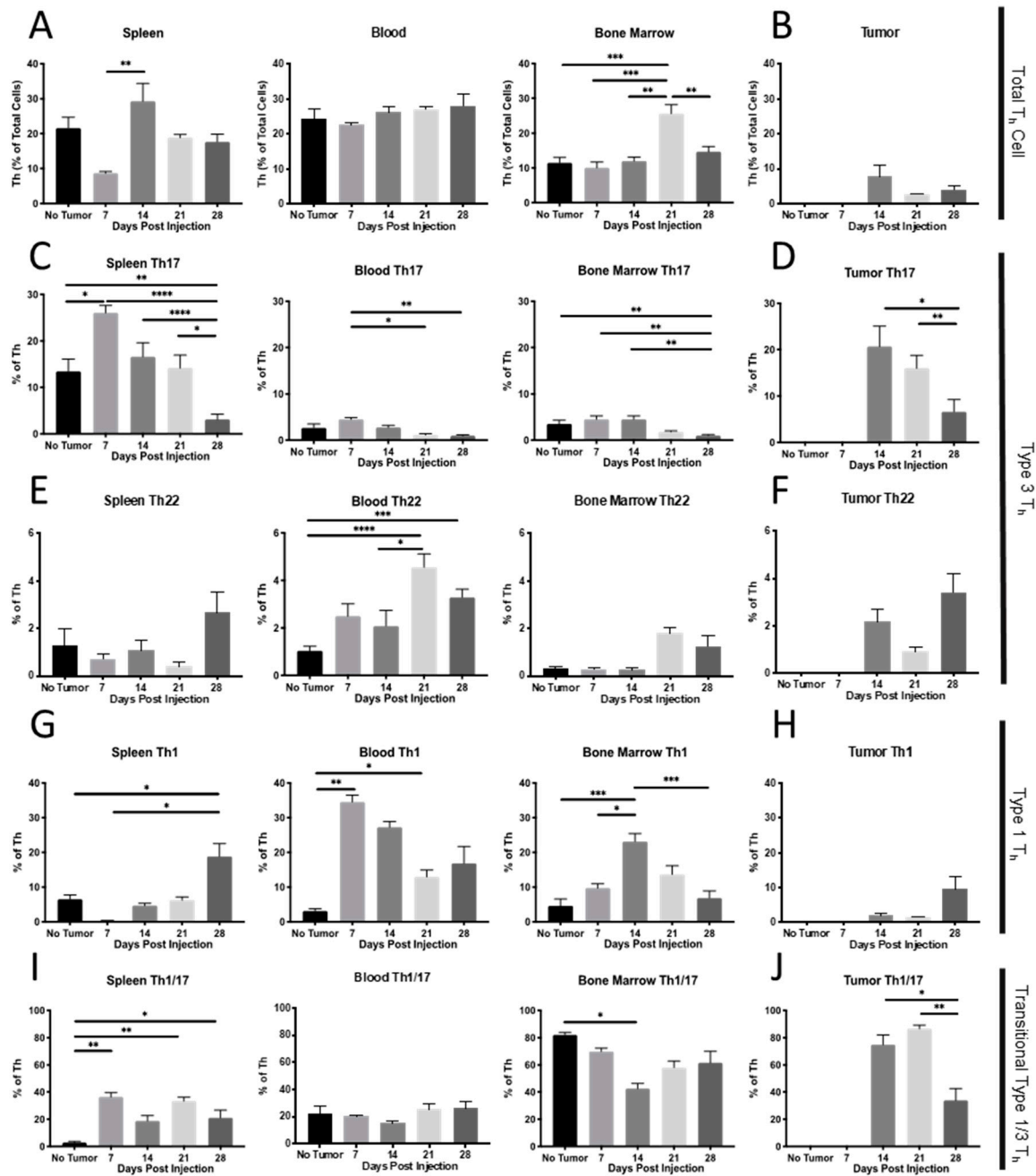
Figure 3. T_h populations over time in 4T1-WT mammary tumor bearing mice. Flow cytometric measurement of total T_h, T_h17, T_h22, T_h1, and $T_h1/17$ in peripheral tissues (**A,C,E,G,I**) or tumors (**B,D,F,H,J**) at the indicated times. Data are presented as mean $\pm$ SEM; n = 4–11 mice per time point. * $p < 0.05$, ** $p < 0.01$, *** $p < 0.001$, and **** $p < 0.0001$.

To look for corresponding changes in the T helper populations, we correlated the proportions of T_h1, T_h17, and T_h22 and found significant negative correlations between T_h1 and T_h17 in the spleen and tumor (Figure 4E,H) but a significant positive correlation in the bone marrow (Figure 4G). When assessing T_h1 vs. T_h22, there was a significant negative correlation between these two cell types in the tumor (Figure 4L). These findings suggest that in the spleen or tumor there is potential for polarization away from type 1 toward a type 3 T_h phenotype, particularly to T_h22. In addition, it may be that the spleen and tumor are conducive to initial T_h activation and polarization (or repolarization), which may explain the relationships in these tissues, but not in blood (Figure 4F,J).
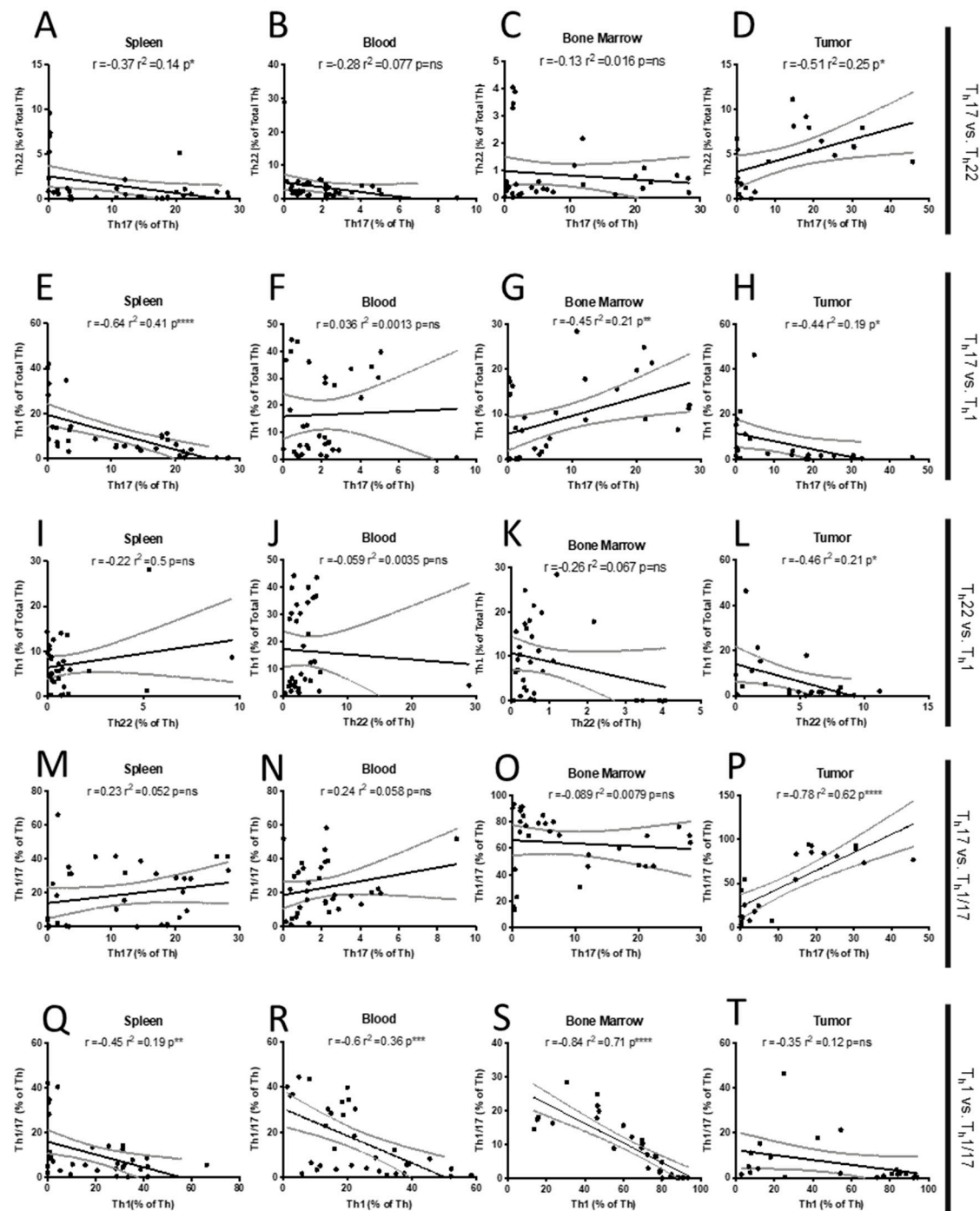
Figure 4. Correlations among T_h subsets in 4T1-WT tumor-bearing mice. Pearson correlations between (**A–D**) T_h17 and T_h22, (**E–H**) T_h17 and T_h1, (**I–L**) T_h22 and T_h1, (**M–P**) T_h17 and $T_h1/17$, (**Q–T**) and T_h1 and $T_h1/17$ levels in spleen, blood, bone marrow, and tumors in 4T1-WT tumor-bearing mice. Simple linear regression and 95% CI are included to help visualize relationships. p = ns (not significant), * $p < 0.05$, ** $p < 0.01$, *** $p < 0.001$, and **** $p < 0.00001$.

Transitional type 1/3 $T_h1/17$ populations. Since we were interested in T_h skewing from type 1 (T_h1) to type 3 (T_h17 and T_h22) or vice versa, we also quantified the $T_h1/17$ transitional population, which represents T_h17 cells transiting to and from an effective, anti-tumor type 1 T_h1 phenotype [45]. In the spleen, $T_h1/17$ were significantly elevated, but were relatively unchanged in blood and bone marrow throughout the time course (Figure 3I). $T_h1/17$ were detectable in the tumor at each time point, with initially higher

levels declining by d 28 (Figure 3J). Given the differentiation plasticity that exists among T_h1, $T_h1/17$, and T_h17, it was interesting that the pattern of tumor-resident $T_h1/17$ and T_h17 was similar across the various time points. This relationship in the tumor was supported by a strongly positive Pearson correlation ($r^2 = 0.62$, **** $p < 0.00001$, Figure 4P); however, a similar relationship was not observed in peripheral organs (Figure 4, M–O). Consistent with differentiation away from the type 1 T_h1 cells toward the type 3 T_h17 phenotype, we saw robust negative correlations between these populations in the spleen ($r^2 = 0.19$, ** $p < 0.001$), blood ($r^2 = 0.36$, *** $p < 0.0001$) and bone marrow ($r^2 = 0.71$, **** $p < 0.00001$; Figure 4Q–S) and a similar non-significant trend in the tumor (Figure 4T).

MDSC expansion and relationship to type 3 T_h17 and T_h22. Type 3 immune responses have been associated with MDSC in other diseases including lupus erythematosus, autoimmune encephalomyelitis, autoimmune arthritis, *H. pylori* infections, and colon cancer [29–31], so we wanted to determine if a similar association might exist in the 4T1 mammary carcinoma model. As expected in tumor-bearing animals [46], MDSC were expanded in the peripheral organs with the M-MDSC and PMN-MDSC subtypes exhibiting similar patterns (Figure 5A,B). In the spleen, MDSC increased progressively over time, while blood MDSC remained low until it increased precipitously during late-stage tumor development (d 28). In the bone marrow, MDSC peaked early at d 7 and then remained significantly elevated above the baseline across all remaining time points. Both M-MDSC and PMN-MDSC were detected in the tumors, but only the PMN-MDSC significantly increased over time (Figure 5A,B).
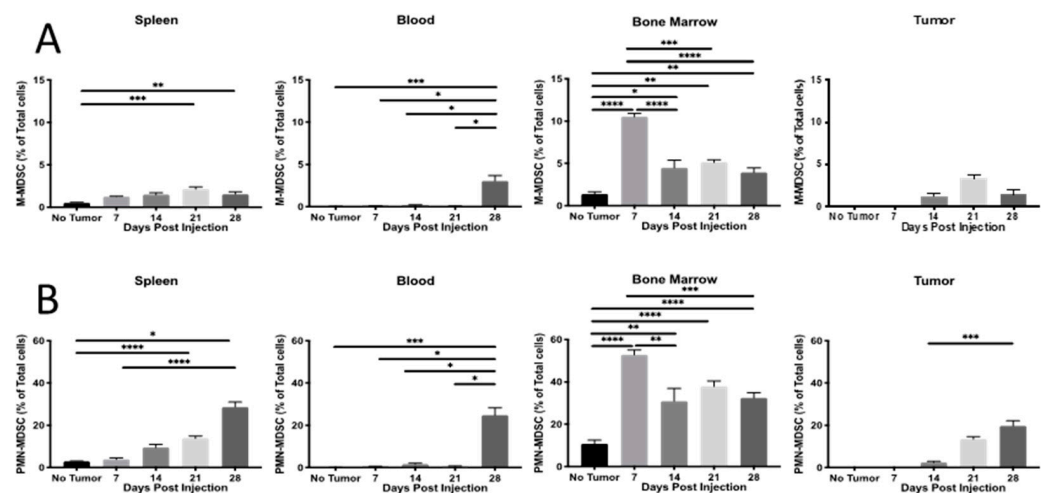

Figure 5. 4T1-WT mammary-tumor-induced MDSC expansion. Flow cytometric measurement of (**A**) M-MDSC and (**B**) PMN-MDSC in response to 4T1-WT mammary tumor development over time. Data are presented as mean ± SEM and n = 4–11 mice per time point. * $p < 0.05$, ** $p < 0.01$, *** $p < 0.001$, and **** $p < 0.0001$.

Again, we used Pearson correlations to compare the patterns of various T_h cell types described in Figure 3 across the time course of MDSC proportions (Figure 6). We observed a very strong positive association between M-MDSC and PMN-MDSC and T_h17 in the bone marrow (Figure 6C,G) but no relationship between T_h22 and MDSC in this tissue (Figure 6K,O). No significant correlations were observed in other tissues, except in blood, where there was an unexpected negative correlation between T_h17 and either PMN- or M-MDSC ($r^2 = 0.21$, * $p < 0.05$, and $r^2 = 0.42$, * $p < 0.05$, respectively; Figure 6B,F).
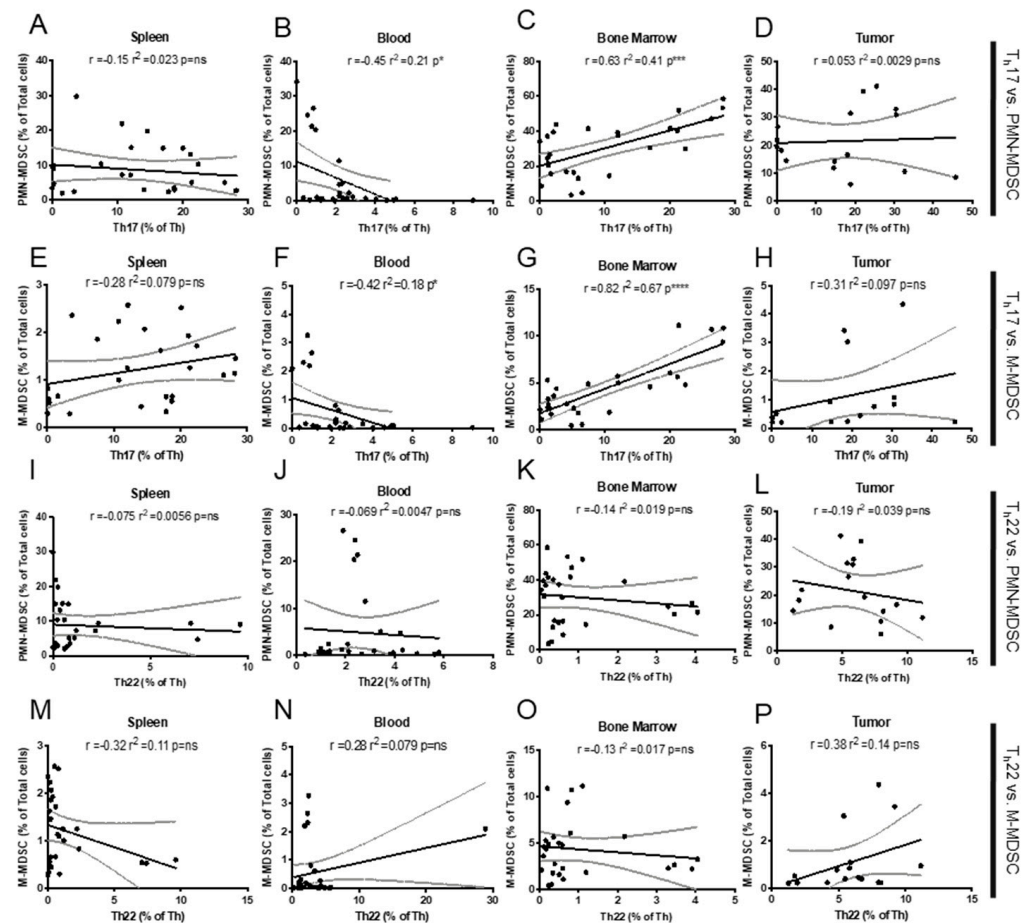
Figure 6. Correlations between type 3 T_h and MDSC accumulation. Pearson correlation assessing the association between type 3 T_h percentages is shown in Figure 3, and MDSC percentages are shown in Figure 5. (**A–D**) T_h17 and PMN-MDSC, (**E–H**) T_h17 and M-MDSC, (**I–L**) T_h22 and PMN-MDSC, and (**M–P**) T_h22 and M-MDSC recruitment in the spleen, blood, bone marrow, and tumor of 4T1 tumor-bearing animals. Simple linear regression included to visualize relationship and 95% CI are presented. p = ns (not significant), * $p < 0.05$, *** $p < 0.001$, and **** $p < 0.00001$.

2.2. Tumor IL-6 Knock Out Effects on Type 3 T_h Cell Recruitment

Tumor IL-6 stimulation of type 3 T_h17 and T_h22 cells. Our time-course data suggested that MDSC and type 3 T_h cells exist at elevated proportions in systemic immunological tissues of tumor-bearing animals, specifically, both MDSC and T_h17 were elevated in blood and bone marrow. Furthermore, there was some indication from the bone marrow that MDSC presence was influencing T_h17 polarization. Collectively, however, there was little direct evidence from the correlative time course studies that MDSC (Figure 5) and the factors driving its recruitment are also responsible for eliciting the observed changes in type 3 T_h populations (Figure 3). Thus, we sought a more direct experimental manipulation to explore potentially linked regulation and the possible interdependence of these cell types. To this end, we noted that others have shown both MDSC and type 3 T_h populations are responsive to circulating IL-6 [33,43], thus we used CRISPR-Cas9 to knock out the IL-6 gene from the 4T1 cell line (4T1-IL6-KO; Figure 7A,B).
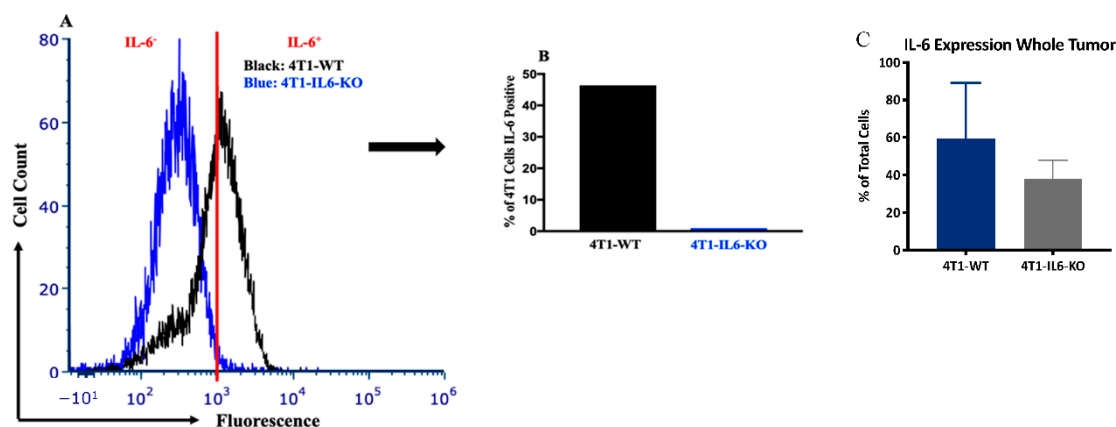
Figure 7. CRISPR/Cas9 knockout of IL-6 in the 4T1 cell line. Wild type 4T1 (4T1-WT) vs. IL-6 knock out 4T1 (4T1-IL6-KO) expression of IL-6 via intracellular flow cytometry. (**A**) Histogram demonstrating relative fluorescence, and (**B**) percentage of total 4T1 that are IL-6 positive. (**C**) Total cells positive for IL-6 in tumors grown from 4T1-WT and 4T1-IL6-KO lines. Background IL-6 positivity in KO tumors likely derives from tumor-associated stromal cells.

Unlike other studies, in which IL-6 is knocked out in the entire animal [47], this approach narrows the IL-6 deficiency to the 4T1 tumor cells responsible for eliciting the MDSC and type 3 T_h responses. Indeed, there remained native stromal and immune cells that continued to express IL-6 in whole tumors (Figure 7C). We did not observe a significant difference in tumor size or mass between the 4T1-WT and 4T1-IL6-KO lines (Figure 8A,B), but, interestingly, spleen mass was significantly higher in 4T1-IL6-KO compared to 4T1-WT animals (Figure 8C).
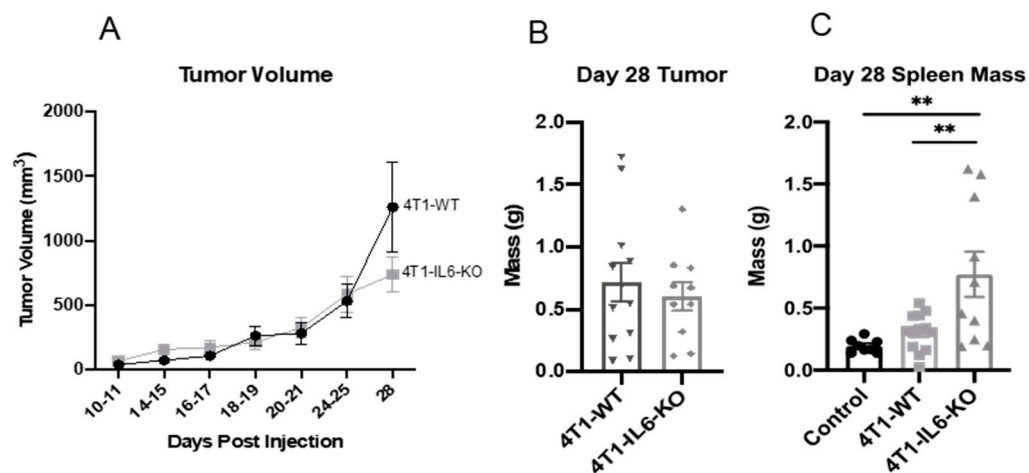

Figure 8. Tumor characteristics and spleen mass in 4T1–WT vs. 4T1–IL6–KO mice. (**A**) The 4T1-WT and 4T1-IL6-KO tumor volumes were measured over time; no statistically significant differences ($p > 0.05$) were detected. (**B**) Final 4T1-WT and 4T1-IL6-KO tumor mass at d 28 post engraftment. (**C**) Spleen mass at d 28 following tumor engraftment; healthy non-tumor-bearing spleens included for reference. The 4T1-IL6-KO spleens were significantly heavier than 4T1-WT and non-tumor-bearing controls. Note that 4T1-IL6-KO is a 4T1-cell-specific IL-6 knockout, not whole animal. ANOVA with Tukey's multiple comparisons. Data are presented as mean $\pm$ SEM and n = 6–11 mice/group. ** $p < 0.01$.

We focused on type 3 cells accumulated at the later d 28 time point, when tumors were well-established. The level of type 3 T_h infiltrating the tumors was intriguing, as 4T1-IL6-KO tumors had expanded T_h17 (Figure 9B), while T_h22 was significantly reduced (Figure 9D). These data suggest that both T_h17 and T_h22 are sensitive to the IL-6 secreted

locally from the tumor cells, but in an opposing fashion. This observation may be in line with the capacity of the tumor microenvironment and its cytokine milieu to re-polarize both the type and subset of T_h cells [16]. In the peripheral tissues, the lack of tumor IL-6 at d 28 reduced $T_h 17$ (Figure 9A), and $T_h 22$ was also lowered (Figure 9C). This suggests that systemically secreted IL-6 from the tumor is necessary to sustain the type 3 T_h immune response outside the tumor.
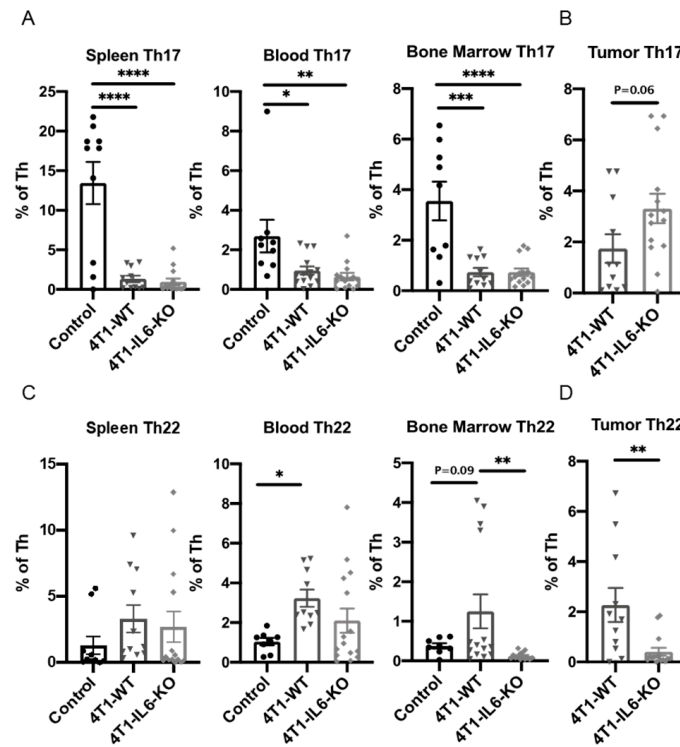

Figure 9. Knocking out tumor cell IL-6 production significantly alters type 3 T helper cell recruitment in the tumor and peripheral tissues. Tumors and peripheral tissues harvested 28 d after engraftment of 4T1-WT and 4T1-IL6-KO cell lines were analyzed for proportions of (**A,B**) $T_h 17$ and (**C,D**) $T_h 22$ type 3 T_h cells. Healthy, non-tumor bearing mice were analyzed for comparison (Control); see Figure 2 for gating strategy. Statistical significance was measured using one-way ANOVA with Tukey's multiple comparisons or Student's t-test. Data are presented as mean $\pm$ SEM with n = 4–11 mice/group. * $p < 0.05$, ** $p < 0.01$, *** $p < 0.001$ and **** $p < 0.0001$.

Tumor IL-6 effects on total T_h, $T_h 1$, $T_h 1/17$, and MDSC. Similar to our earlier time course study, we examined other T_h and MDSC populations in the 4T1-IL6-KO model at d 28. It is worth noting that the response of these cell populations could be viewed as indicators of how clinically depleting tumor IL-6 with targeted agents such as tocilizumab could influence the efficacy of checkpoint immunotherapies. For example, the proportion of total T_h cells was significantly increased in the blood and tumors of 4T1-IL6-KO tumor-bearing mice (Figure 10), an effect that could prove beneficial if translated to the oncology clinic. Levels of $T_h 1/17$ and $T_h 1$ were variable across the tissues and treatment groups (Figure 11). We saw $T_h 1/17$ significantly expanded in the blood and tumor of the 4T1-IL6-KO animals (Figure 11A), while $T_h 1$ was significantly increased in the spleen but significantly decreased in the blood of 4T1-IL6-KO tumor-bearing mice (Figure 11B).
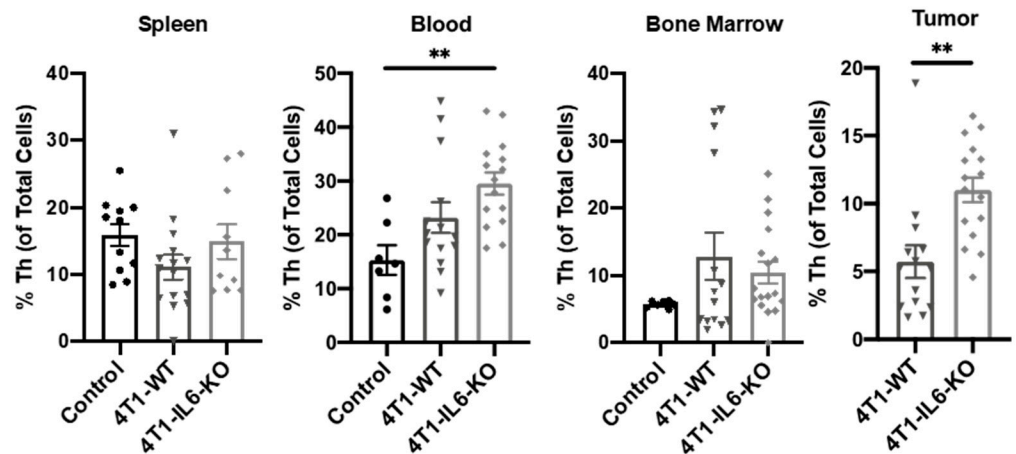
Figure 10. Knocking out tumor cell IL-6 production increases tumor-infiltrating CD3$^+$/CD4$^+$ T helper cells. Tumors and peripheral tissues harvested 28 d after engraftment of 4T1-WT and 4T1-IL6-KO cell lines were analyzed for total CD3$^+$CD4$^+$ T$_h$ cells. Healthy, non-tumor-bearing mice were analyzed for comparison (control); see Figure 2 for gating strategy. Data are presented as mean $\pm$ SEM; n = 4–11 mice/group. ** $p < 0.01$.

Figure 11. Depleting tumor cell IL-6 increases tumor-infiltrating T$_h$1/17 cells. Tumors and peripheral tissues harvested 28 d after engraftment of 4T1-WT and 4T1-IL6-KO cell lines were analyzed for proportions of (**A**) T$_h$1/17 and (**B**) T$_h$1 subtype T helper cells. Healthy, non-tumor-bearing mice were analyzed for comparison (control); see Figure 2 for gating strategy. Data are presented as mean $\pm$ SEM; n = 4–11 mice/group. * $p < 0.05$, ** $p < 0.01$.
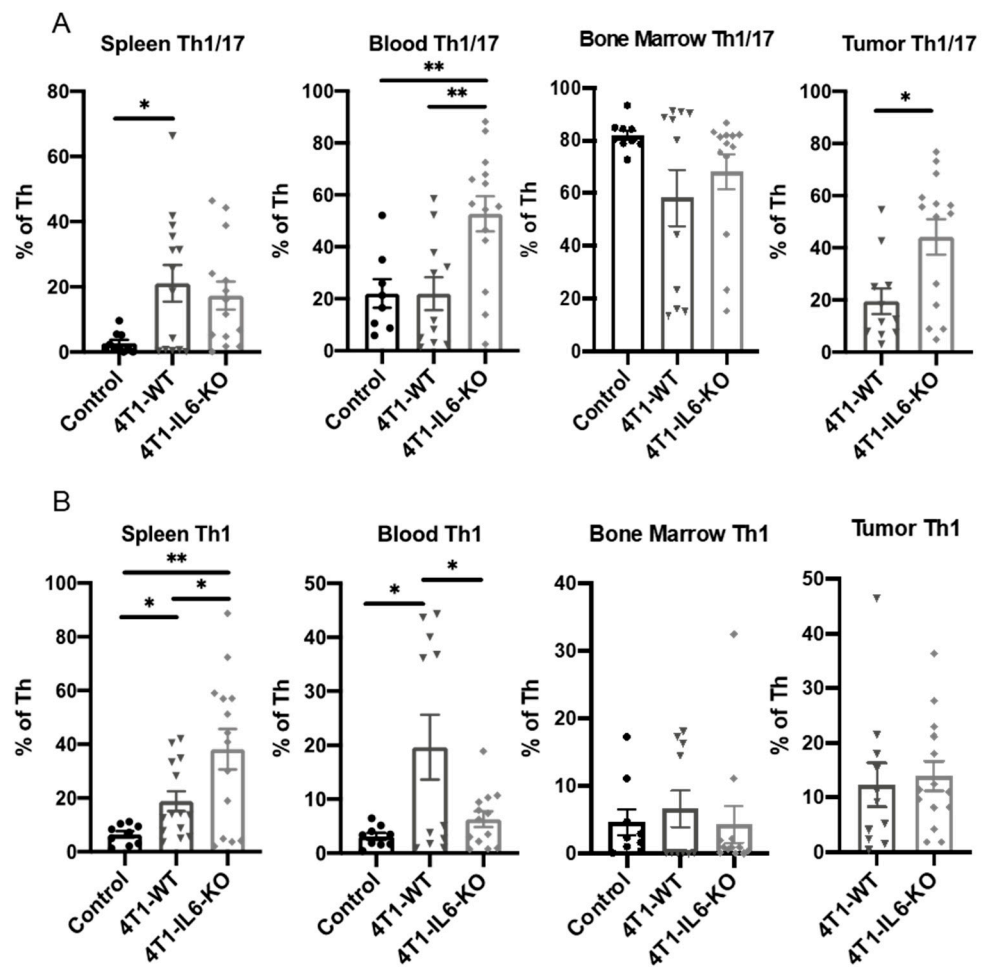
The 4T1-specific knockout of IL-6 led to a significant reduction in both M-MDSC and PMN-MDSC in all peripheral organs (Figure 12A,C), and tumor=-infiltrating M-MDSC was also reduced in the 4T1-IL6-KO tumors (Figure 12B). This further supports the idea that tumor-derived IL-6 promotes MDSC expansion [43] and that blocking systemic IL-6 signaling could prove beneficial to cancer patients, so it should be further explored. Relating this decline in MDSC back to the concurrent changes in type 3 T_h populations, there is again some evidence that MDSC may be similarly regulated and perhaps responsible for changes in the T_h22 populations, as these patterns very closely mirror each other in the IL-6 KO condition. However, any associated changes in T_h17 did not parallel the reduced MDSC population, suggesting independent regulation of this T_h subtype.
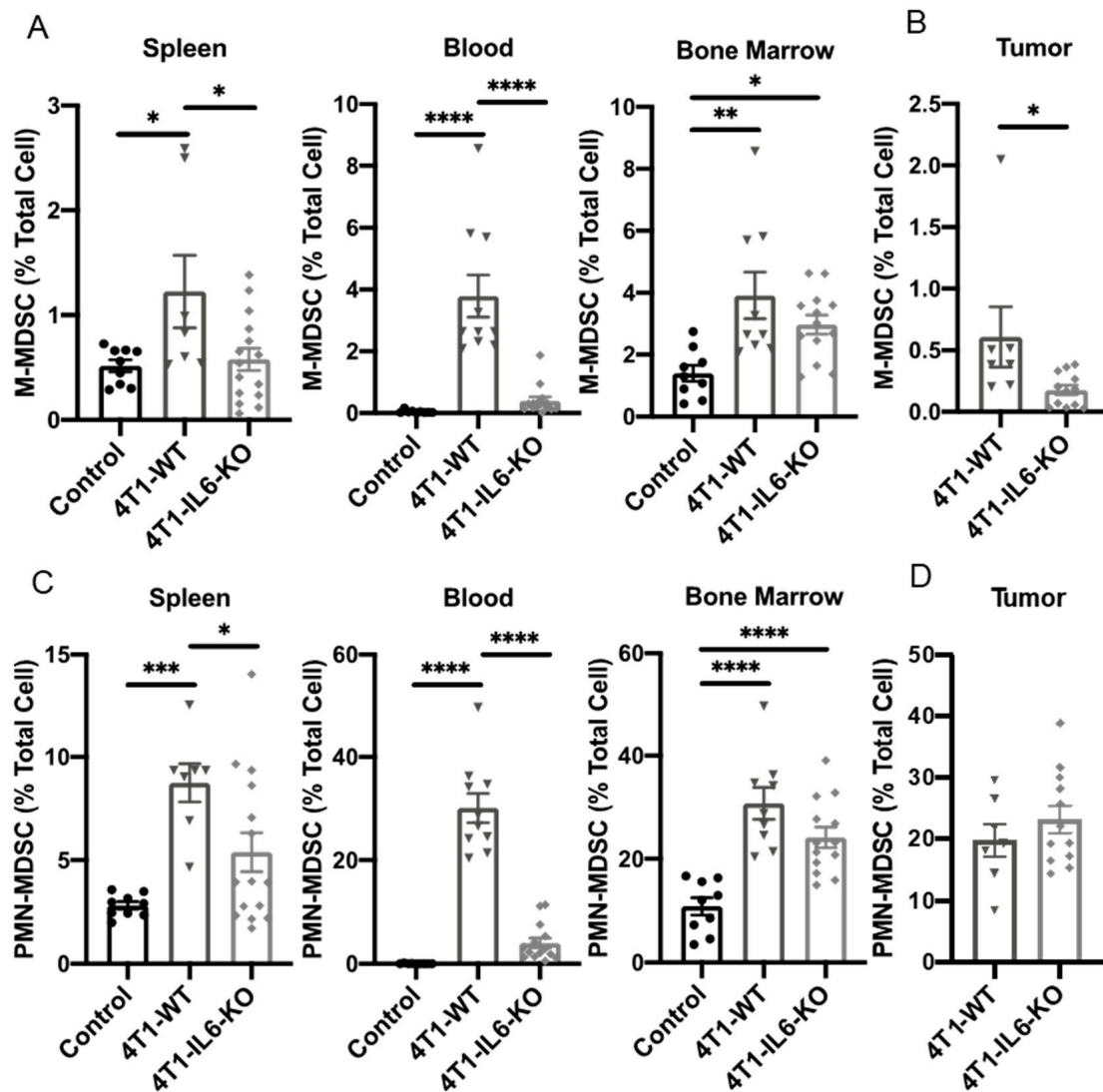
Figure 12. Knocking out tumor cell IL-6 production significantly reduces M-MDSC and PMN-MDSC recruitment. Tumors and peripheral tissues harvested 28 d after engraftment of 4T1-WT and 4T1-IL6-KO cell lines were analyzed for proportions of (**A**,**B**) M-MDSC and (**C**,**D**) PMN-MDSC. Healthy, non-tumor-bearing mice were analyzed for comparison (control); see Figure 2 for gating strategy. Data are presented as mean ± SEM; n = 4–11 mice/group. * $p < 0.05$, ** $p < 0.01$, *** $p < 0.001$, and **** $p < 0.0001$.

3. Discussion

Our data support a model (graphical abstract) in which mammary tumors repurpose secreted IL-6 and other cytokines to act locally and systemically in reshaping normal T_h

and myeloid immunity. This influence occurs quickly, as we found that type 3 T_h17 and T_h22 cell populations, which are more commonly associated with extracellular microbial infection [48], were recruited before formation of a visible or palpable mass, within 7 d of injecting 10^4 cells (Figure 3). We have yet to determine if these early responses are IL-6-dependent, as our 4T1-IL6-KO studies focused on late-stage tumor development. As tumors become more established, the type 3 immune response appears to switch from a predominantly T_h17 response to a T_h22 response, and this switch is again driven in part by IL-6 (Figure 9) and likely other cytokines. The distinct timing and pattern of T_h17 vs. T_h22 recruitment reinforces that these are indeed distinct T_h lineages. Our data support previous work showing that tumor IL-6 impacts myelopoiesis and MDSC [43], but importantly it also positions tumor-derived IL-6 as a negative regulator of the total $CD4^+$ T_h cell population, an effect that is particularly pronounced locally in the tumor (Figure 10). Additional grafting studies are required to determine whether there are direct interactions between MDSC and type 3 T_h immune cells.

Implications of type 3 polarization in breast cancer. Our preclinical findings suggest that mammary tumors may elicit a type 3 T_h immune reaction, with the potential to diminish initial immune surveillance and ultimately reduce the efficacy of immunotherapies, including checkpoint inhibitors. While the 4T1 model is known to resist checkpoint therapies [49], further experiments are needed to determine the role played by polarization to pro-tumor type 2 (T_h2) [50] or type 3 (T_h17 or T_h22) cells in this resistance. As others have suggested [16,51], a type 3 T_h immune response is expected to support tumor growth, while distracting away from an effective type 1 response. In the context of checkpoint-inhibitor treatment, T cell clonal expansion followed by polarization is possible; however, it remains to be seen which antigens these T_h cells recognize. It may be that they do not recognize tumor-specific neoantigen displayed on MHC and are merely bystanders, but, again, the pro-tumor attributes ascribed to these populations suggests otherwise. For example, T_h22 cells may facilitate metastasis in high-grade breast cancer via IL-22 [52,53]. Moreover, IL-22 is known to promote wound healing in the skin and gastrointestinal tract and has been shown to promote mouse mammary cancer growth [28], all suggesting that this cytokine may support a breast tumor microenvironment and provide aid for the growth of malignant cells [35,54]. The 4T1 tumor model is representative of metastatic, high-grade breast cancer [40,41], which shows robust T_h22 recruitment as time progresses (Figure 3). While tumor growth was similar with reduced T_h22 in the 4T1-IL6-KO, the potential effects of T_h22 and, by extension, IL-22 on metastatic burden warrant further study [35]. In addition to IL-22, we observed $IL-17^+$ T_h17 cells. We found that T_h17 cells appeared to be present in high proportions in the bone marrow and tumor. This illustrates the necessity to further investigate the clinical consequences of recruited type 3 immunity in breast cancer.

MDSC. The pro-tumor activities of these immature myeloid cells have been well-established [32,43,55,56]. In our time course study, early MDSC expansion in the bone marrow was followed by progressive increases in the spleen, suggesting gradual splenic takeover of MDSC maintenance (Figure 5A,B). The initial expansion of MDSC in the bone marrow is logical as this is the presumed tissue of origin, but it is remarkable that the MDSC increase was detectable very early (first sampling at d 7 post-engraftment), before a tumor can be visualized. A similar MDSC increase was seen in the spleen beginning on day 7, and it is interesting to note that the spleen mass is significantly lower than in non-tumor-bearing controls at this point, which might suggest substantial immune remodeling within the spleen before the tumor mass is established and splenomegaly ensues (Figure 5). A better understanding of these dynamic MDSC changes in human cancers could someday help inform clinicians about the stage of disease progression and the immune context of proposed cancer treatments [32].

It remains unclear, in the context of cancer, whether there are direct functional interactions between MDSC and type 3 immune cells. We saw varying correlations among these cell populations depending on cell and tissue type (Figure 7B,C,F,G). Speculating based on timing, our data may suggest that early MDSC in the bone marrow, which gas

not acquired conventional suppressive capacity [57,58], may still be capable of locally influencing polarization toward type 3 T_h17 responses, before leaving to mature in the spleen. While more studies are needed to confirm this relationship, this would be an additional novel mechanism by which MDSC could deplete the type 1 immune response and facilitate tumor progression. This speculative mechanism aligns with research in rheumatoid arthritis where MDSC promote T_h17 responses, but are unable to suppress effector T_h to halt an autoimmune reaction [31]. Previously our lab has verified that both M-MDSC ($CD11b^+Ly-6G^-Ly-6C^{hi}$) and PMN-MDSC ($CD11b^+Ly-6G^+Ly-6C^{low}$) recruited in the 4T1 model of breast cancer are T-cell-suppressive, beginning at d 28 post tumor injection [59]. This suggests that MDSC may have some other functional significance to the tumor before acquiring direct suppressive capacity, which may be recruitment of pro-tumor type 3 immune cells.

Polarization to type 1 immunity. We assessed recruitment of $T_h1/17$ as a potential indicator of polarization from type 3 to the more beneficial type 1 immunity. The T_h17 phenotype has been shown to be more plastic than the T_h1 phenotype, and it is thought that $T_h1/17$ represent cells transiting away from T_h17 toward the T_h1 phenotype [60]. Our data support this previous work, as we saw a robust and significant positive correlation between the presence of T_h17 and $T_h1/17$ in the tumor (Figure 4P). The lack of a similar correlation in peripheral tissues suggests, paradoxically, that the tumor microenvironment itself may be uniquely re-polarizing the immune response. We also noted negative correlations between T_h1 and $T_h1/17$ in peripheral tissues (Figure 4Q–T), further suggesting movement from type 3 to a type 1 immunity as $T_h1/17$ polarize to replenish exhausted T_h1 populations. Additionally, there was a rise in tumor T_h1 at later time points (Figure 3H), which could reflect $T_h1/17$ transiting toward T_h1. It should be explored further whether the tumor specific milieu of cells and cytokines could be manipulated to encourage a unidirectional T_h17 to $T_h1/17$ to T_h1 conversion, as this could be therapeutically beneficial. Nevertheless, it is difficult to rule out polarization from type 1 to type 3 immunity, as this would logically benefit the tumor. Consistent with this directionality are the negative correlations observed between both T_h1 and T_h17 and T_h1 and T_h22 in the spleen and tumor. We did not specifically examine which population of T_h cells (T_h1 or T_h17) was actively undergoing clonal expansion, but, again, based on previous work [60], we speculate that $T_h1/17$ likely originate from T_h17 and not T_h1.

Tumor-cell-specific IL-6 knockout. We were interested in determining the mechanism underlying the changes in type 3 T_h and MDSC in the 4T1-WT time course studies described above. We focused on tumor-derived IL-6 expression for multiple reasons: (1) it can act as an immunosuppressive, pro-tumor cytokine expressed by 4T1 cells [61,62]; (2) it is a known driver of MDSC expansion [32]; (3) it has been implicated in type 3 immunity in other systems [51]; and (4) there exist IL-6-specific, FDA-approved monoclonal antibodies, tocilizumab and siltuximab, to treat rheumatoid arthritis [63] and Castleman disease [64], respectively. By using CRISPR to knock out IL-6 in the 4T1 cell line (4T1-IL6-KO), a unique opportunity was provided to evaluate the effect of excess IL-6 originating specifically from the tumor cells. Again, samples obtained from whole tumor tissue show that abundant stromal IL-6 expression accompanies the 4T1-IL6-KO cells (Figure 7C).

When assessing tumor-resident T_h17 and T_h22 in the 4T1-IL6-KO, T_h17 was expanded, whereas T_h22 was significantly reduced, consistent with other reports that IL-6 is a key cytokine determinate of both type 3 lineages [33]. However, IL-6 appears to be necessary but not sufficient to discriminate between these lineages, as the residual populations of these cells points to additional regulatory factors. One such factor is TGF-β1, which is thought to be a primary determinant of T_h17 or T_h22 polarization [33]. We did not assess whether the IL-6 KO altered TGF-β1 expression, but our data do suggest that the source and concentration of IL-6 influences T_h22 or T_h17 skewing. This is a mechanism that should be examined further, as there is little information on IL-6 source, TGF-β1 signaling, and IL-6 receptor expression in these type 3 cells or the other local constituents with which they would interact.

While growth of the tumors was not impacted, 4T1-IL6-KO was associated with several immune effects that could be beneficial, if translatable to the oncology clinic. First, we saw a reduction in tumor resident T_h22, a primary source of IL-22 that has been implicated in promoting growth and metastasis of various cancer types [65]. Reduced IL-6 from tumor cells also led to increased tumor-infiltrating T_h17 and IFN-γ positive $T_h1/17$, supporting the notion that these cells may be transitioning from T_h17 to a T_h1 phenotype; however, it is important to note that these cells may also give rise to T_{reg} [60,66,67], which were not assessed in the present study. Furthermore, we observed a reduction in M-MDSC across all tissues, including tumor tissues, and a significant reduction in PMN-MDSC in all peripheral organs. Indeed, this was our initial prediction and impetus for the IL-6 portion of the study. Other studies have shown that depletion of MDSC with guadecitabine encourages anti-tumor T-cell-mediated immunity, suggesting that the removal of MDSC alone is enough to bolster T cell-mediated immunotherapy [68,69]. Finally, and perhaps most unexpectedly and remarkably, was that 4T1-IL6-KO was associated with an increased total of CD4$^+$ T_h cells in the tumors and blood. We are unaware of any other reports indicating that tumor-derived IL-6 could have such a broad, suppressive (or distractive) effect on T_h populations. Again, this and the other preclinical observations discussed above strongly support further exploration of IL-6-lowering monoclonal antibodies in the clinical oncology setting, with particular consideration given to combining these agents with checkpoint inhibitors and other type 1-dependent immunotherapies.

Limitations. We acknowledge that this study has potential limitations, some of which we highlight here. Foremost, we did not follow up our study with a complete IL-6 knockout mouse. This means that other infiltrating stromal and immune cells were a source of IL-6; our goal, herein, was strictly to eliminate cancer-cell-derived IL-6. Similarly, we did not examine serum levels of IL-6 or other cytokines during development of these tumors, since targeting systemic IL-6 was not the objective of this study. Nevertheless, this could provide further insight on the effects tumoral IL-6 has in this model. Based on our data, we suggest that there are meaningful systemic changes in the cellular immune response to the removal of tumoral IL-6. Further, the nature of direct interactions, or the lack thereof, between the MDSC and type 3 T_h subsets will require manipulation studies directed at this question. While the trends between MDSC and T_h17 and T_h22 in the tumor are not significant, both co-exist in time and location, raising the possibility of reciprocal influence. Finally, we limited the scope of our study to the tracking of specific T_h subsets and MDSC, therefore, we do not know if any other changes to other immune cells occurred; given the broad influence of the T_h compartment over homeostasis, it is reasonable to hypothesize that other cellular parameters were affected. Additionally, given this was an observational study that did not investigate the functional consequences of type 3 immunity in tumors, it remains unclear as to whether the subsets play a consequential role in tumor growth by interacting with MDSC in peripheral organs. However, this work serves—to our knowledge—as one of the first to highlight the presence of type 3 immune cells in the 4T1 system. This should be considered when evaluating the immune system wholistically, whilst designing immunotherapeutic strategies in the presence of malignant disease.

In sum, this study demonstrated that there is a dynamic pro-tumor type 3 immune response in reaction to 4T1 mammary carcinoma. Furthermore, the effects of tumor-derived IL-6 on the tumor and peripheral immune landscapes were explored. It was found that knocking out tumor IL-6 significantly increased tumor-infiltrating T_h cells, significantly increased IFN-γ producing $T_h1/17$, and reduced MDSC recruitment. These results demonstrate that IL-6 should be considered a therapeutic target in select circumstances where aberrant type 3 immune skewing is involved, which may better facilitate an initial, appropriate anti-tumor immune response.

4. Methods and Materials

4.1. Mice and 4T1 Mammary Tumors

The 4T1 cells were purchased from ATCC (Manassas, VA, USA) and cultured in RPMI 1640 (ThermoFisher, Waltham, MA, USA) supplemented with 1% pen/strep, 2 mM L-Glutamine, 1 mM Sodium Pyruvate, 10 mM HEPES, 0.05 mM β-mercaptoethanol, and 10% (by volume) FB Essence (VWR, Radnor, PA, USA). To grow syngeneic, orthotopic mammary tumors, female BALB/cJ mice (Jackson Laboratory, Bar Harbor, ME, USA) between four to six weeks of age were inoculated with 1.0×10^4 4T1 cells. Cells were washed and suspended in 100 μL 1X HBSS (Ca^{2+}/Mg^{2+} free, ThermoFisher) before injection through the nipple of the upper-right mammary fat pad using an insulin syringe. Mice were monitored daily for availability of food and water and any signs or symptoms of peripheral infection or inflammation. Palpable tumors were routinely detected 2 weeks after injection, and tumor sizes were monitored by calipers. Final tumor volumes were calculated by volume = $(3.14/6)$width $\times$ length^2 [70]. In the 4T1 tumor time-course study, tissues were harvested at days 0, 7, 14, 21, and 28 post-injection (Figure 2A). On the day of tissue harvest, mice were euthanized by CO_2 asphyxiation and tumors weighed before further processing. All animal procedures were performed according to approved Institutional Animal Care and Use Committee protocols (numbers: 1906CE-RH-RM-22 and 1702C-NP-M-20).

4.2. il6 Gene Knock-Out in 4T1 Cells

The CRISPR/Cas9 system was used to generate 4T1 cells deficient in IL-6 (4T1-IL6-KO). Guide RNAs (gRNA) were designed with CRISPOR software (http://crispor.tefor.net/, version 5.01 as of publication date, by Jean-Paul Concordet and Maximilian Haeussler, Santa Cruz, CA, USA, accessed on 15 April 2019) to target exon 2 of the *Mus musculus il6* gene (GenBank: M24221.1) at sequence TATACCACTTCACAAGTCGG. The gRNA oligos (Invitrogen, Carlsbad, CA, USA) were annealed, phosphorylated, and cloned into the pX458 vector following the Zhang lab protocol [71]. The vector pSpCas9(BB)-2A-GFP (PX458) was a gift from Feng Zhang (Addgene plasmid number 48138, Watertown, MA, USA). Plasmids were transfected using Lipofectamine 3000 (ThermoFisher). The vector includes a green fluorescent protein (GFP) reporter, and GFP$^+$ cells were single-cell sorted into 96-well plates using a Sony SH800 Cell Sorter (Sony Biotechnology, San Jose, CA, USA). Subclones were cultured, and IL-6 deficiency was verified by fixed-cell intracellular flow cytometry with IL-6 antibody (BioLegend, #504504, San Diego, CA, USA). Two independent subclones verified subsequently as GFP-negative, IL-6 knockouts were pooled to create the 4T1-IL6-KO line used in these studies.

4.3. Tissue Processing

Spleens were weighed, dissected, and dissociated in 500 μL of 1X HBSS. Blood was collected from the chest cavity, following a cut to the aorta and local heparin infusion. Blood was centrifuged at $200\times g$ for 10 min, and buffy coat and plasma were transferred to fresh vials, before lysing residual red blood cells with ACK lysis buffer (Quality Biological, Gaithersburg, MD, USA). Bone marrow was flushed from excised femurs and tibias using HBSS. Final tumor sizes were measured prior to excision, and tumors were weighed after excision and removal of extraneous tissue. Tumor tissue was minced and mechanically separated using a cell dissociation sieve fitted with a 100 μm mesh screen and resuspended in 1 mL HBSS. Cells were resuspended in type IV collagenase (2 mg/1 mL) and DNase (0.1 mg/mL; Worthington Biochemical, Lakewood, NJ, USA) and then incubated at 37 °C rocking at 225 rpm for 1 h. Remaining erythrocytes from various tissues were cleared with ACK lysis buffer.

4.4. Flow Cytometry and Antibodies

Cells were stained in flow cytometry buffer: 0.5% BSA in Ca^{2+}/Mg^{2+} free 1X Dulbecco's PBS (ThermoFisher). Flow reagents and antibodies were purchased from BioLegend (San Diego, CA, USA), unless stated otherwise, and catalog numbers of critical antibody

reagents are included for reproducibility. Fc block (#101302) was used prior to staining with extracellular markers, in accordance with the protocol of the manufacturer. Any surface marker staining was performed prior to fixation with buffer (#420801), in accordance with the recommendation of the manufacturer. For intracellular markers, prior to cell surface staining and fixation, cells were treated with 1X brefeldin A (#420601) for 3–4 h at 37 °C to block intracellular protein trafficking. Cells were then stained for surface markers, fixed and permeabilized with buffer (#421002), and finally stained for intracellular targets, in accordance with the protocol of the manufacturer. Samples were analyzed using an Attune NxT cytometer (ThermoFisher); raw data were processed in FCS Express version 6 (De Novo Software, Pasadena, CA, USA).

The biomarker profiles used to define cell types in these studies were as follows: M-MDSC (CD11b$^+$Ly-6G$^-$Ly-6C^{hi}), PMN-MDSC (CD11b$^+$Ly-6G$^+$Ly-6C^{low}), T$_h$17 (CD3$^+$CD4$^+$ RORγt$^+$IFN-γ^-IL-17A$^+$IL-22$^{+/-}$), T$_h$1/17 (CD3$^+$CD4$^+$RORγt$^+$IFN-γ^+IL-17A$^+$IL-22$^{+/-}$), T$_h$1 (CD3$^+$CD4$^+$IFN-γ^+RORγt$^-$IL-17A$^-$IL-22$^{+/-}$), and T$_h$22 (CD3$^+$CD4$^+$IFN-γ^-RORγt$^-$IL-17A$^-$IL-22$^+$). Antibodies for these markers included CD3 (#100237), CD4 (#100438), MDSC antibody cocktail (#77496), IFNγ (#505806), IL-22 (#516409), IL-17A (#506904), and RORγt, which were from ThermoFisher (#46698180). An example of flow cytometric gating strategy is presented in Figure 2B,C.

4.5. Statistical Analyses

All data are presented as mean $\pm$ SEM, and statistical tests used $\alpha = 0.05$. Grubbs' test was used to identify outliers. All multiple comparisons were calculated using one-way ANOVA with Tukey's multiple comparisons test. Single comparisons were calculated using Student's t-test. A simple linear regression and Pearson's correlation were used to assess the relationships between cell types in the 4T1-WT time course study; for each of these regressions, animals across all time points were included. A confidence interval (CI) of 95% is represented as well as Pearson r and r^2 values, with significance set by $\alpha = 0.05$. All statistical analyses were conducted in Prism 8 (GraphPad, San Diego, CA, USA). R^2 (coefficient of determination) and r (Pearson correlation coefficient) values are used to predict the relationship between independent and dependent variables in a linear model. R represents the overall strength and direction of a correlation, while r^2 is indicative of how well the data fit to a regression line. R values are measured from -1 to $+1$; 0 indicates no relationship. R^2 is measured from 0 to $+1$, while 0 indicates the model explains none of the variability [72].

Abbreviations

CTLA-4	cytotoxic T-lymphocyte-associated protein 4
G-CSF	granulocyte colony-stimulating factor
IFN	interferon
IL	interleukin
M-CSF	macrophage colony-stimulating factor
MDSC	myeloid-derived suppressor cell
MHS	major histocompatibility complex
M-MDSC	mononuclear MDSC
PD-1/PD-L1	programmed cell death protein 1/programmed death ligand 1
PMN-MDSC	polymorphonuclear MDSC
TGF	transforming growth factor
T_h	T helper lymphocyte
TIL	Tumor-infiltrating lymphocyte

References

1. Ansell, S.M.; Lesokhin, A.M.; Borrello, I.; Halwani, A.; Scott, E.C.; Gutierrez, M.; Schuster, S.J.; Millenson, M.M.; Cattry, D.; Freeman, G.J.; et al. PD-1 blockade with nivolumab in relapsed or refractory Hodgkin's lymphoma. *N. Engl. J. Med.* **2015**, *372*, 311–319. [CrossRef] [PubMed]
2. Herbst, R.S.; Soria, J.-C.; Kowanetz, M.; Fine, G.D.; Hamid, O.; Gordon, M.S.; Sosman, J.A.; McDermott, D.F.; Powderly, J.D.; Gettinger, S.N.; et al. Predictive correlates of response to the anti-PD-L1 antibody MPDL3280A in cancer patients. *Nature* **2014**, *515*, 563–567. [CrossRef]
3. Topalian, S.L.; Taube, J.M.; Anders, R.A.; Pardoll, D.M. Mechanism-driven biomarkers to guide immune checkpoint blockade in cancer therapy. *Nat. Cancer* **2016**, *16*, 275–287. [CrossRef]
4. Hamid, O.; Robert, C.; Daud, A.; Hodi, F.S.; Hwu, W.J.; Kefford, R.; Wolchok, J.D.; Hersey, P.; Joseph, R.; Weber, J.S.; et al. Five-year survival outcomes for patients with advanced melanoma treated with pembrolizumab in KEYNOTE-001. *Ann. Oncol. Off. J. Eur. Soc. Med. Oncol.* **2019**, *30*, 582–588. [CrossRef]
5. Tan, D.S.W. Changing the natural history of non–small-cell lung cancer through upfront programmed death protein 1/programmed death-ligand 1 blockade. *J. Clin. Oncol.* **2017**, *35*, 2735–2736. [CrossRef]
6. Kanjanapan, Y.; Day, D.; Wang, L.; Al-Sawaihey, H.; Abbas, E.; Namini, A.; Siu, L.L.; Hansen, A.; Razak, A.A.; Spreafico, A.; et al. Hyperprogressive disease in early-phase immunotherapy trials: Clinical predictors and association with immune-related toxicities. *Cancer* **2019**, *125*, 1341–1349. [CrossRef]
7. Frelaut, M.; Le Tourneau, C.; Borcoman, E. Hyperprogression under immunotherapy. *Int. J. Mol. Sci.* **2019**, *20*, 2674. [CrossRef] [PubMed]
8. Sama, S.; Hadfield, M.J.; Lia, N.L.; Vredenburgh, J. Hyperprogression in PDL1 expressive, recurrent gastroesophageal-junction adenocarcinoma after pembrolizumab. *Cureus* **2019**, *11*, e4862. [CrossRef]
9. Champiat, S.; Dercle, L.; Ammari, S.; Massard, C.; Hollebecque, A.; Postel-Vinay, S.; Chaput, N.; Eggermont, A.; Marabelle, A.; Soria, J.C.; et al. Hyperprogressive disease is a new pattern of progression in cancer patients treated by anti-PD-1/PD-L1. *Clin. Cancer Res.* **2017**, *23*, 1920–1928. [PubMed]
10. Saâda-Bouzid, E.; Defaucheux, C.; Karabajakian, A.; Coloma, V.P.; Servois, V.; Paoletti, X.; Even, C.; Fayette, J.; Guigay, J.; Loirat, D.; et al. Hyperprogression during anti-PD-1/PD-L1 therapy in patients with recurrent and/or metastatic head and neck squamous cell carcinoma. *Ann. Oncol. Off. J. Eur. Soc. Med. Oncol.* **2017**, *28*, 1605–1611. [CrossRef] [PubMed]
11. Swoboda, A.; Nanda, R. Immune checkpoint blockade for breast cancer. *Cancer Treat. Res.* **2018**, *173*, 155–165. [CrossRef] [PubMed]
12. Dai, M.; Hellstrom, I.; Yip, Y.Y.; Sjögren, H.O.; Hellstrom, K.E. Tumor regression and cure depends on sustained Th1 responses. *J. Immunother.* **2018**, *41*, 369–378. [CrossRef]
13. Castro, F.; Cardoso, A.P.; Gonçalves, R.M.; Serre, K.; Oliveira, M.J. Interferon-gamma at the crossroads of tumor immune surveillance or evasion. *Front. Immunol.* **2018**, *9*, 847. [CrossRef]
14. Coffelt, S.B.; de Visser, K.E. Immune-mediated mechanisms influencing the efficacy of anticancer therapies. *Trends Immunol.* **2015**, *36*, 198–216.
15. Capasso, A.; Lang, J.; Pitts, T.M.; Jordan, K.R.; Lieu, C.H.; Davis, S.L.; Diamond, J.R.; Kopetz, S.; Barbee, J.; Peterson, J.; et al. Characterization of immune responses to anti-PD-1 mono and combination immunotherapy in hematopoietic humanized mice implanted with tumor xenografts. *J. Immunother. Cancer* **2019**, *7*, 37. [CrossRef] [PubMed]
16. Jiao, S.; Subudhi, S.K.; Aparicio, A.; Ge, Z.; Guan, B.; Miura, Y.; Sharma, P. Differences in tumor microenvironment dictate t helper lineage polarization and response to immune checkpoint therapy. *Cell* **2019**, *179*, 1177–1190.e13. [CrossRef] [PubMed]
17. Kang, X.; Zhang, X.; Liu, Z.; Xu, H.; Wang, T.; He, L.; Zhao, A. Granulocytic myeloid-derived suppressor cells maintain feto-maternal tolerance by inducing Foxp3 expression in CD4 + CD25 − T cells by activation of the TGF-β/β-catenin pathway. *Mol. Hum. Reprod.* **2016**, *22*, 499–511. [CrossRef] [PubMed]

18. Alspach, E.; Lussier, D.M.; Miceli, A.P.; Kizhvatov, I.; DuPage, M.; Luoma, A.M.; Meng, W.; Lichti, C.F.; Esaulova, E.; Vomund, A.N.; et al. MHC-II neoantigens shape tumour immunity and response to immunotherapy. *Nature* **2019**, *574*, 696–701. [CrossRef] [PubMed]

19. Bianco, T.M.; Abdalla, D.R.; Desidério, C.S.; Thys, S.; Simoens, C.; Bogers, J.-P.; Murta, E.F.; Michelin, M.A. The influence of physical activity in the anti-tumor immune response in experimental breast tumor. *Immunol. Lett.* **2017**, *190*, 148–158. [CrossRef] [PubMed]

20. Zhang, Q.; Qin, J.; Zhong, L.; Gong, L.; Zhang, B.; Zhang, Y.; Gao, W.-Q. CCL5-Mediated Th2 immune polarization promotes metastasis in luminal breast cancer. *Cancer Res.* **2015**, *75*, 4312–4321. [CrossRef]

21. Kidd, P. Th1/Th2 balance: The hypothesis, its limitations, and implications for health and disease. *Altern. Med. Rev.* **2003**, *8*, 223–246. [PubMed]

22. Wu, H.; Zhen, Y.; Ma, Z.; Li, H.; Yu, J.; Xu, Z.-G.; Wang, X.-Y.; Yi, H.; Yang, Y.-G. Arginase-1–dependent promotion of Th17 differentiation and disease progression by MDSCs in systemic lupus erythematosus. *Sci. Transl. Med.* **2016**, *8*, 331ra40. [CrossRef] [PubMed]

23. Gillentine, M.A.; Berry, L.N.; Goin-Kochel, R.P.; Ali, M.A.; Ge, J.; Guffey, D.; Rosenfeld, J.A.; Hannig, V.; Bader, P.; Proud, M.; et al. Myeloid-derived suppressor cells have a proinflammatory role in the pathogenesis of autoimmune arthritis. *J. Autism. Dev. Disord.* **2017**, *47*, 549–562. [CrossRef]

24. Glenn, J.D.; Liu, C.; Whartenby, K.A. Induction of experimental autoimmune encephalomyelitis mobilizes Th17-promoting myeloid derived suppressor cells to the lung. *J. Leukoc. Biol.* **2019**, *105*, 829–841.

25. Lim, C.; Savan, R. The role of the IL-22/IL-22R1 axis in cancer. *Cytokine Growth Factor Rev.* **2014**, *25*, 257–271. [PubMed]

26. Zhang, W.; Tian, X.; Mumtahana, F.; Jiao, J.; Zhang, T.; Della Croce, K.; Ma, D.; Kong, B.; Cui, B. The existence of Th22, pure Th17 and Th1 cells in CIN and Cervical Cancer along with their frequency variation in different stages of cervical cancer. *BMC Cancer* **2015**, *15*, 717. [CrossRef] [PubMed]

27. Housseau, F.; Geis, A.; Thiele-Orberg, E.; Llosa, N. Interleukin-17 and type 17 helper T cells in cancer management and research. *ImmunoTargets Ther.* **2014**, *3*, 39–54. [CrossRef]

28. Zhang, Y.; Liu, C.; Gao, J.; Shao, S.; Cui, Y.; Yin, S.; Pan, B. IL-22 promotes tumor growth of breast cancer cells in mice. *Aging* **2020**, *12*, 13354–13364. [CrossRef]

29. Zhuang, Y.; Cheng, P.; Liu, X.-F.; Peng, L.-S.; Li, B.-S.; Wang, T.-T.; Chen, N.; Li, W.-H.; Shi, Y.; Chen, W.; et al. A pro-inflammatory role for Th22 cells in *Helicobacter pylori*-associated gastritis. *Gut* **2014**, *64*, 1368–1378. [CrossRef]

30. Wegner, A.; Verhagen, J.; Wraith, D.C. Myeloid-derived suppressor cells mediate tolerance induction in autoimmune disease. *Immunology* **2017**, *151*, 26–42. [CrossRef]

31. Jayakumar, A.; Bothwell, A.L.M. Functional diversity of myeloid-derived suppressor cells: The multitasking hydra of cancer. *J. Immunol.* **2019**, *203*, 1095–1103. [CrossRef]

32. Veglia, F.; Perego, M.; Gabrilovich, D. Myeloid-derived suppressor cells coming of age review-article. *Nat. Immunol.* **2018**, *19*, 108–119. [CrossRef] [PubMed]

33. Plank, M.W.; Kaiko, G.E.; Maltby, S.; Weaver, J.; Tay, H.L.; Shen, W.; Wilson, M.S.; Durum, S.K.; Foster, P.S. Th22 Cells form a distinct TH lineage from th17 cells in vitro with unique transcriptional properties and TBET-dependent th1 plasticity. *J. Immunol.* **2017**, *198*, 2182–2190. [CrossRef]

34. Eyerich, K.; DiMartino, V.; Cavani, A. IL-17 and IL-22 in immunity: Driving protection and pathology. *Eur. J. Immunol.* **2017**, *47*, 607–614. [CrossRef]

35. Zenewicz, L.A. IL-22: There Is a Gap in Our Knowledge. *ImmunoHorizons* **2018**, *2*, 198–207. [CrossRef]

36. Vitiello, G.A.; Miller, G. Targeting the interleukin-17 immune axis for cancer immunotherapy. *J. Exp. Med.* **2019**, *217*, e20190456. [CrossRef]

37. Nam, J.-S.; Terabe, M.; Kang, M.-J.; Chae, H.; Voong, N.; Yang, Y.-A.; Laurence, A.; Michalowska, A.; Mamura, M.; Lonning, S.; et al. Transforming growth factor β subverts the immune system into directly promoting tumor growth through interleukin-17. *Cancer Res.* **2008**, *68*, 3915–3923. [CrossRef] [PubMed]

38. Jiang, M.; Chen, J.; Zhang, W.; Zhang, R.; Ye, Y.; Liu, P.; Yu, W.; Wei, F.; Ren, X.; Yu, J. Interleukin-6 trans-signaling pathway promotes immunosuppressive myeloid-derived suppressor cells via suppression of suppressor of cytokine signaling 3 in breast cancer. *Front. Immunol.* **2017**, *8*, 1840. [CrossRef] [PubMed]

39. Chatterjee, S.; Daenthanasanmak, A.; Chakraborty, P.; Wyatt, M.; Dhar, P.; Selvam, S.P.; Fu, J.; Zhang, J.; Nguyen, H.; Kang, I.; et al. CD38-NAD+Axis regulates immunotherapeutic anti-tumor T cell response. *Cell Metab.* **2018**, *27*, 85–100.e8. [CrossRef]

40. Grasselly, C.; Denis, M.; Bourguignon, A.; Talhi, N.; Mathe, D.; Tourette, A.; Serre, L.; Jordheim, L.P.; Matera, E.L.; Dumontet, C. The antitumor activity of combinations of cytotoxic chemotherapy and immune checkpoint inhibitors is model-dependent. *Front. Immunol.* **2018**, *9*, 2100. [CrossRef]

41. Castle, J.C.; Loewer, M.; Boegel, S.; Tadmor, A.D.; Boisguerin, V.; De Graaf, J.; Paret, C.; Diken, M.; Kreiter, S.; Türeci, Ö.; et al. Mutated tumor alleles are expressed according to their DNA frequency. *Sci. Rep.* **2014**, *4*, 4743. [CrossRef]

42. Bunt, S.K.; Yang, L.; Sinha, P.; Clements, V.K.; Leips, J.; Ostrand-Rosenberg, S. Reduced inflammation in the tumor microenvironment delays the accumulation of myeloid-derived suppressor cells and limits tumor progression. *Cancer Res.* **2007**, *67*, 10019–10026. [CrossRef]

43. Talmadge, J.E.; Gabrilovich, D.I. History of myeloid-derived suppressor cells. *Nat. Cancer* **2013**, *13*, 739–752. [CrossRef] [PubMed]

44. Dupre', S.A.; Hunter, K.W. Murine mammary carcinoma 4T1 induces a leukemoid reaction with splenomegaly: Association with tumor-derived growth factors. *Exp. Mol. Pathol.* **2007**, *82*, 12–24. [CrossRef]

45. Harbour, S.N.; Maynard, C.L.; Zindl, C.L.; Schoeb, T.R.; Weaver, C.T. Th17 cells give rise to Th1 cells that are required for the pathogenesis of colitis. *Proc. Natl. Acad. Sci. USA* **2015**, *112*, 7061–7066. [CrossRef]

46. Bosiljcic, M.; Cederberg, R.A.; Hamilton, M.J.; LePard, N.E.; Harbourne, B.T.; Collier, J.L.; Halvorsen, E.C.; Shi, R.; Franks, S.E.; Kim, A.Y.; et al. Targeting myeloid-derived suppressor cells in combination with primary mammary tumor resection reduces metastatic growth in the lungs. *Breast Cancer Res.* **2019**, *21*, 103. [CrossRef] [PubMed]

47. Chang, Q.; Bournazou, E.; Sansone, P.; Berishaj, M.; Gao, S.P.; Daly, L.; Wels, J.; Theilen, T.; Granitto, S.; Zhang, X.; et al. The IL-6/JAK/Stat3 Feed-forward loop drives tumorigenesis and metastasis. *Neoplasia* **2013**, *15*, 848–862, IN40–IN45. [CrossRef]

48. Mühl, H.; Bachmann, M.; Pfeilschifter, J. Inducible NO synthase and antibacterial host defence in times of Th17/Th22/T22 immunity. *Cell. Microbiol.* **2011**, *13*, 340–348. [CrossRef]

49. De Henau, O.; Rausch, M.; Winkler, D.; Campesato, L.F.; Liu, C.; Cymerman, D.H.; Budhu, S.; Ghosh, A.; Pink, M.; Tchaicha, J.; et al. Overcoming resistance to checkpoint blockade therapy by targeting PI3Kγ in myeloid cells. *Nature* **2016**, *539*, 443–447. [CrossRef]

50. Mandal, P.K.; Biswas, S.; Mandal, G.; Purohit, S.; Gupta, A.; (Giri), A.M.; Chowdhury, S.R.; Bhattacharyya, A. CCL2 conditionally determines CCL22-dependent Th2-accumulation during TGF-β-induced breast cancer progression. *Immunobiology* **2018**, *223*, 151–161. [CrossRef]

51. Annunziato, F.; Romagnani, C.; Romagnani, S. The 3 major types of innate and adaptive cell-mediated effector immunity. *J. Allergy Clin. Immunol.* **2015**, *135*, 626–635. [CrossRef] [PubMed]

52. Wang, T.; Zhang, Z.; Xing, H.; Wang, L.; Zhang, G.; Yu, N.; Wang, J.; Guo, W.; Jiang, J. Elevated Th22 cells and related cytokines in patients with epithelial ovarian cancer. *Medicine* **2017**, *96*, e8359. [CrossRef]

53. Wang, S.; Yao, Y.; Yao, M.; Fu, P.; Wang, W. Interleukin-22 promotes triple negative breast cancer cells migration and paclitaxel resistance through JAK-STAT3/MAPKs/AKT signaling pathways. *Biochem. Biophys. Res. Commun.* **2018**, *503*, 1605–1609. [CrossRef] [PubMed]

54. Arnold, K.M.; Opdenaker, L.M.; Flynn, D.; Sims-Mourtada, J. Wound healing and cancer stem cells: Inflammation as a driver of treatment resistance in breast cancer. *Cancer Growth Metastasis* **2015**, *8*, CGM.S11286-13. [CrossRef]

55. Bronte, V.; Brandau, S.; Chen, S.-H.; Colombo, M.P.; Frey, A.B.; Greten, T.F.; Mandruzzato, S.; Murray, P.J.; Ochoa, A.; Ostrand-Rosenberg, S.; et al. Recommendations for myeloid-derived suppressor cell nomenclature and characterization standards. *Nat. Commun.* **2016**, *7*, 12150. [CrossRef]

56. Ostrand-Rosenberg, S.; Sinha, P.; Figley, C.; Long, R.; Park, D.; Carter, D.; Clements, V.K. Frontline science: Myeloid-derived suppressor cells (MDSCs) facilitate maternal–fetal tolerance in mice. *J. Leukoc. Biol.* **2016**, *101*, 1091–1101. [CrossRef]

57. Gabrilovich, D.I. Myeloid-derived suppressor cells. *Cancer Immunol. Res.* **2017**, *5*, 3–8. [CrossRef]

58. Ortiz, M.L.; Kumar, V.; Martner, A.; Mony, S.; Donthireddy, L.; Condamine, T.; Seykora, J.; Knight, S.C.; Malietzis, G.; Lee, G.H.; et al. Immature myeloid cells directly contribute to skin tumor development by recruiting IL-17–producing CD4+ T cells. *J. Exp. Med.* **2015**, *212*, 351–367. [CrossRef] [PubMed]

59. Garritson, J.; Krynski, L.; Haverbeck, L.; Haughian, J.M.; Pullen, N.A.; Hayward, R. Physical activity delays accumulation of immunosuppressive myeloid-derived suppressor cells. *PLoS ONE* **2020**, *15*, e0234548. [CrossRef] [PubMed]

60. Guéry, L.; Hugues, S. Th17 cell plasticity and functions in cancer immunity. *BioMed Res. Int.* **2015**, *2015*, 314620. [CrossRef]

61. Fisher, D.T.; Appenheimer, M.M.; Evans, S.S. The two faces of IL-6 in the tumor microenvironment. *Semin. Immunol.* **2014**, *26*, 38–47. [CrossRef]

62. Zhang, W.; Jiang, M.; Chen, J.; Zhang, R.; Ye, Y.; Liu, P.; Yu, W.; Yu, J. SOCS3 suppression promoted the recruitment of CD11b+Gr-1-F4/80-MHCII- early-stage myeloid-derived suppressor cells and accelerated interleukin-6-related tumor invasion via affecting myeloid differentiation in breast cancer. *Front. Immunol.* **2018**, *9*, 1699. [CrossRef] [PubMed]

63. Actemra (Tocilizumab) for Intravenous Infusion. Genentech. January 2010. Available online: http://www.gene.com/gene/products/information/actemra/pdf/pi.pdf (accessed on 1 July 2022).

64. Sitenga, J.; Aird, G.; Ahmed, A.; Silberstein, P.T. Impact of siltuximab on patient-related outcomes in multicentric Castleman's disease. *Patient Relat. Outcome Meas.* **2018**, *9*, 35–41. [CrossRef]

65. Zhuang, Y.; Peng, L.-S.; Zhao, Y.-L.; Shi, Y.; Mao, X.-H.; Guo, G.; Chen, W.; Liu, X.-F.; Zhang, J.-Y.; Liu, T.; et al. Increased intratumoral IL-22-producing CD4+ T cells and Th22 cells correlate with gastric cancer progression and predict poor patient survival. *Cancer Immunol. Immunother.* **2012**, *61*, 1965–1975. [CrossRef]

66. Wu, X.; Tian, J.; Wang, S. Insight into non-pathogenic Th17 Cells in autoimmune diseases. *Front. Immunol.* **2018**, *9*, 1112. [CrossRef] [PubMed]

67. Song, X.; Sun, X.; Oh, S.F.; Wu, M.; Zhang, Y.; Zheng, W.; Geva-Zatorsky, N.; Jupp, R.; Mathis, D.; Benoist, C.; et al. Microbial bile acid metabolites modulate gut RORγ+ regulatory T cell homeostasis. *Nature* **2020**, *577*, 410–415. [CrossRef]

68. Anani, W.; Shurin, M.R. Targeting myeloid-derived suppressor cells in cancer. In *Advances in Experimental Medicine and Biology*; Springer New York LLC.: New York, NY, USA, 2017; Volume 1036, pp. 105–128.

69. Luker, A.J.; Graham, L.J.; Smith, T.M.; Camarena, C.; Zellner, M.P.; Gilmer, J.-J.S.; Damle, S.R.; Conrad, D.H.; Bear, H.D.; Martin, R.K. The DNA methyltransferase inhibitor, guadecitabine, targets tumor-induced myelopoiesis and recovers T cell activity to slow tumor growth in combination with adoptive immunotherapy in a mouse model of breast cancer. *BMC Immunol.* **2020**, *21*, 8. [CrossRef]

70. Faustino-Rocha, A.; Oliveira, P.A.; Pinho-Oliveira, J.; Teixeira-Guedes, C.; Soares-Maia, R.; da Costa, R.G.; Colaço, B.; Pires, M.J.; Colaço, J.; Ferreira, R.; et al. Estimation of rat mammary tumor volume using caliper and ultrasonography measurements. *Lab. Anim.* **2013**, *42*, 217–224. [CrossRef]

71. Cong, L.; Ran, F.A.; Cox, D.; Lin, S.; Barretto, R.; Habib, N.; Hsu, P.D.; Wu, X.; Jiang, W.; Marraffini, L.A.; et al. Multiplex genome engineering using CRISPR/Cas systems. *Science* **2013**, *339*, 819–823. [CrossRef]

72. Kasuya, E. On the use of r and r squared in correlation and regression. *Ecol. Res.* **2019**, *34*, 235–236. [CrossRef]